JOURNAL OF SPACECRAFT AND ROCKETS
Vol. 29, No. 2, March-April 1992

Thermal Design Verification of a Large Deployable Antenna for a Communications Satellite

H. Tsunoda,* K. Nakajima,† and A. Miyasaka‡
NTT Radio Communication Systems Laboratories,
Yokosuka, Kanagawa 238-03, Japan

A large deployable antenna for a communication satellite requires sophisticated thermal control to satisfy the temperature requirements for electrical characteristics, and its performance must be confirmed by a thermal balance test. The results of a tradeoff study of the thermal control method for an antenna conducted in an effort to meet temperature requirement demands indicate that the thermal design of an antenna system can be accomplished by using passive thermal control techniques and heaters in spite of the large and complicated structure. Antenna system thermal balance tests are limited by the volume of the space simulation chamber. To overcome this problem, we introduce a two-step thermal design verification method consisting of component level tests and a whole antenna system level test. This paper describes the thermal control method, the thermal design verification method, and the predicted antenna temperatures in a geostationary orbit obtained from the verified thermal analytical model.

Introduction

FUTURE multibeam communication satellites will require antenna systems that are larger and more complex than the currently popular horn reflector-type antenna. To stow such large antenna systems in the fairing of the launch vehicle, they must be equipped with deployable reflectors and a tower-type antenna configuration must be adopted to mount the antenna reflectors and the feed components.[1] The large deployable antenna also requires a high-accuracy lightweight reflector in order to satisfy the electrical characteristics for ensuring both gain and beam pointing accuracy. The main-reflector structure in which the main reflector is supported by many studs on the truss tube can satisfy these requirements. The antenna thermal design must not only maintain the component temperatures but must also minimize the weight and power consumption of the thermal control subsystem. One tradeoff study of the thermal control method for large antenna reflectors was reported by Benton,[2] but the configuration of the antenna system was too simple. In this work, a tradeoff study of the thermal control method by conventional passive thermal control techniques and heaters for a complex antenna system is conducted in order to meet these requirements.

Based on the thermal balance tests, thermal analytical models of satellite antennas must be verified to insure temperature predictions in space environments, even if the size is much larger than a conventional single-beam antenna.[3] The thermal design and testing of Intelsat-V spacecraft were reported by Spencer et al.[4] However, thermal balance tests for such a large antenna system are limited by the volume of the space simulation chamber. In addition, the deployment mechanisms cannot support the reflector without suffering damage due to the gravitational conditions on the ground. As a result, the utilization of a large antenna system makes it difficult to conduct a thermal balance test for a geosynchronous orbit configuration.

To overcome these problems, we introduce a two-step thermal design verification method. First, thermal analytical models of the antenna components are verified using the results of the thermal balance tests conducted on each component under critical component temperature conditions. These results enable us to evaluate the thermal capacity and the internal thermal conductances for radiation and conduction. Next, a thermal analytical model of the antenna system is verified using the results of the antenna system thermal balance tests conducted for typical test cases. These results enable us to confirm the thermal coupling between each antenna component, the interface temperatures, and the external heat input values. The antenna system thermal balance tests were performed using the supporting structures that support the hard points of each main reflector to minimize the effects of gravity on the antenna deployment mechanisms.

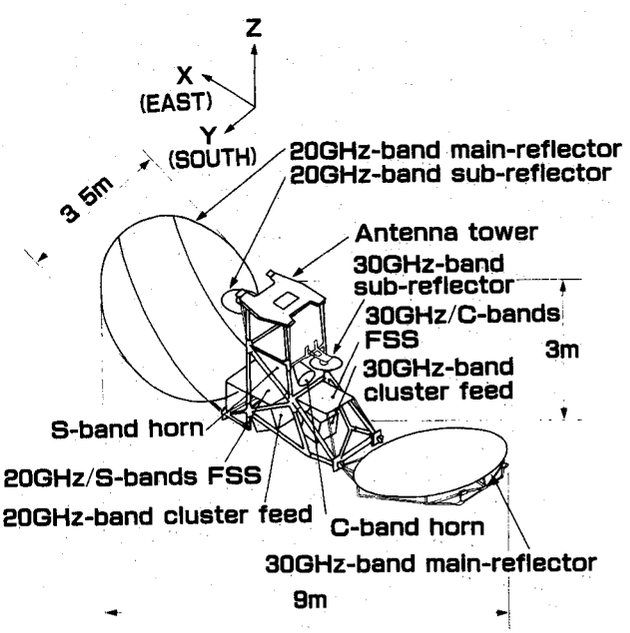

Fig. 1 Antenna system configuration.

Received May 2, 1991; presented as Paper 91-1301 at the AIAA 26th Thermophysics Conference, Honolulu, HI, June 24-26, 1991; revision received Sept. 9, 1991; accepted for publication Sept. 11, 1991.

*Senior Research Engineer, Satellite Communication Systems Laboratory, 1-2356 Take. Member AIAA
†Senior Research Engineer, Supervisor. Member AIAA.
‡Research Engineer.

Antenna Configuration and Thermal Control

Antenna Configuration and Thermal Control Requirements

The selected antenna system configuration is a tower-mounted type, as illustrated in Fig. 1. The system has a total length of about 9 m and is comprised of 2.5- and 3.5-m-diam main reflectors, subreflectors fitted with antenna pointing mechanisms (APMs), Ka-band (20- and 30-GHz bands) cluster feeds, a C-band horn, an S-band horn, frequency selective surfaces (FSSs) to enable simultaneous reflector use for different bands, and an antenna tower for mounting on the three-axis stabilized satellite.[1] For the transfer and drift orbits, the main and subreflectors are positioned adjacent to the antenna tower. To satisfy beam pointing accuracy requirements and to obtain the structural quality necessary for the thermal vacuum environment of space, thermal control for the satellite antenna must be optimized to satisfy the temperature limits of each antenna component listed in Table 1.

Thermal Control Method

In this section, the thermal control method of each antenna component and a tradeoff study of the thermal control method for the main reflectors and the antenna tower are discussed.

Main Reflectors

Although the surface area of the main reflector is 10 times larger than that of a conventional horn-type reflector, high surface accuracy and lightweight reflectors are required in order to use 20/30-GHz-band missions. Therefore, sandwich panel-type dishes supported by truss structures through studs were developed.

Two thermal configurations were considered for the main reflectors. The first was to coat them with white paint on the front side and wrap the backside with multilayer insulation (MLI) blankets. The other design used the basic thermo-optical properties of the carbon fiber reinforced plastics (CFRP) surfaces. The surface accuracy of the reflector is influenced by the shadow on the reflector, which changes during a 24-h period, as shown in Fig. 2. This figure, which was obtained for the 30-GHz-band main reflector, shows that the magnitude of the thermal distortion becomes large when the antenna tower or the satellite bus casts a shadow on the reflector. However, the thermal distortion, which is caused by the shadow of the satellite bus, can be decreased by the combination of white paint and MLI blankets. This is because the maximum temperature and temperature gradient are decreased due to the low absorptivity of white paint and the thermal coupling between the backside of the reflector, the truss tube, and the inner side of the MLI blankets.

Table 1 Antenna temperature limits, °C

Components	Nonoperational	Operational
Main reflectors and subreflectors	−180 ~ +100	−180 ~ +100
20-GHz-band cluster feed	−110 ~ + 95	− 30 ~ + 75
30-GHz-band cluster feed	−120 ~ + 95	− 50 ~ + 25
S-band horn	−145 ~ + 95	−105 ~ + 80
C-band horn	−150 ~ + 95	− 80 ~ + 60
20-GHz/S-bands FSS	−150 ~ + 95	−140 ~ + 60
30-GHz/C-bands FSS	−160 ~ + 95	−145 ~ + 70
APMs	− 40	~ + 90
Deployment mechanisms	− 90	~ +100

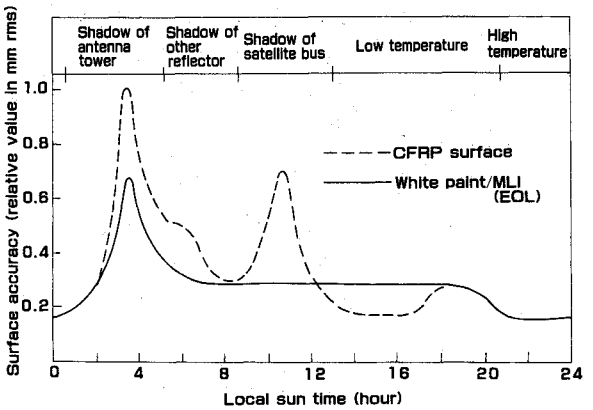

Fig. 2 Thermal distortion excursions of reflector surface.

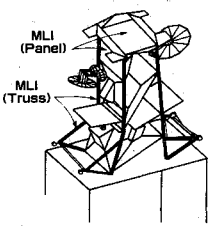

a) Configuration A—tower trusses wrapped with MLI

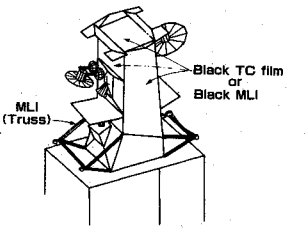

b) Configuration B—tower covered with black TC films; configuration C—tower covered with black MLI

Fig. 3 Thermal configurations tradeoff of antenna tower.

Subreflectors

Each subreflector is attached to an APM that utilizes heaters for temperature control. To minimize heater power consumption, the backsides of the APMs and the subreflectors are wrapped with MLI blankets and the front surfaces are coated with white paint.

Antenna Tower and Feed Components[5]

Although the antenna tower is made of CFRP, which has low thermal expansion, the relative positions of each antenna component are affected by the thermal distortions of the tower. Furthermore, the temperature ranges of the components inside the tower and the reflectors depend on the thermal configuration of the tower. These factors led us to carry out the tradeoff study to clarify the relation between the tower configuration and the component temperatures.

The configurations considered for the antenna tower were trusses wrapped with MLI blankets (configuration A), the tower completely covered with black thin films (configuration B), and the tower completely covered with black MLI blankets (configuration C). These configurations are illustrated in Fig. 3. In configurations B and C, black thin polyimide films were selected to avoid the multireflections among the films, main reflector, and subreflector surfaces. These three thermal configurations were selected because the estimated differences in weight between them were less than 1 kg, which is negligible compared with the weight of the antenna system.

Some results of the tradeoff study are shown in Fig. 4. The temperatures were obtained from a steady-state analysis considering the sunlit conditions at 6 a.m., 12 noon, 9 p.m., and 12 a.m. local sun time. Configuration C was chosen because the results revealed that the temperature variations of the cluster feeds, of which thermal deformations are the most critical, were controlled within smaller ranges.

The thermal design for the feed components was also determined in accordance with the establishment of the thermal configuration of the tower. During the geostationary orbit

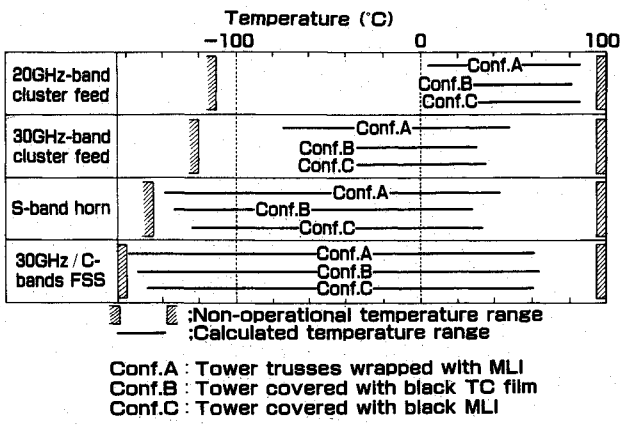

Fig. 4 Feed component temperatures as a function of tower configurations.

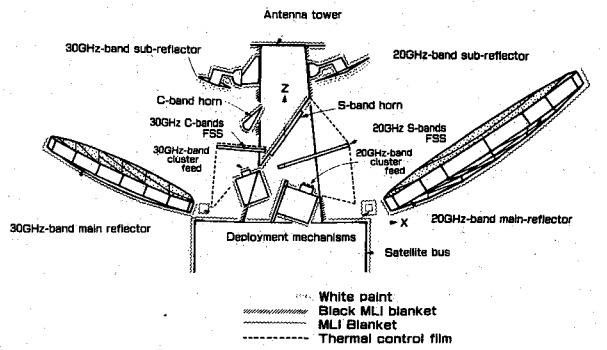

Fig. 5 Thermal configuration of antenna module.

phase, temperature variations of the feed components must be kept as small as possible to minimize thermal deformations and associated pointing errors. Therefore, the ray-path portions were covered with thin thermal control (TC) films and the other areas were wrapped with MLI blankets. The thermal configuration of the antenna module is presented in Fig. 5. As shown in this figure, TC films were not placed over the front surface of the S-band horn to reduce the rf losses.

Thermal Control Material

The thermal control material properties are summarized in Table 2. Since only a thin (about 30 μm) coat of white paint is required, its weight is only half that of a coat of conventional silicon alkyd resins-type paint.[6] The TC film consists of a polyimide film adhered to a polyvinyl fluoride film, and its solar absorptivity has a low degradation characteristic. Ten-layer MLI blankets are used for the APMs and the deployment mechanisms in order to minimize the heater power consumption required to control the temperatures. On the other hand, three-layer MLI blankets are used for the backsides of the main reflectors and the antenna tower to block sunlight, maintain truss tube temperatures uniformly, and minimize the weight of the thermal control materials. A carbon-filled polyimide film with vacuum-deposited aluminum on the backside, which is used to coat the outer layers of the black MLI blankets, has a heat-resistant temperature characteristic of 288°C, which is sufficient for continuous use.

Thermal Design Verification Method

Thermal balance tests, which are conducted for a geostationary orbit configuration, are important ways for verifying the thermal analytical model and evaluate the thermal design of the onboard antenna system. However, the deployed antenna is quite large (about 9.0 × 3.5 m) and the deployment mechanisms cannot support the reflectors without suffering damage caused by the gravitational condition on the ground. Therefore, thermal balance tests cannot provide useful test cases for the thermal design evaluation of all antenna components. To overcome this problem, we introduced the two-step thermal design verification method shown in Fig. 6 to verify the thermal analytical model for temperature predictions in a geostationary orbit.

First, thermal analytical models of the antenna components were verified using the results of the thermal balance tests conducted on each component under critical component temperature conditions. Using these results, we were able to evaluate the thermal capacity and the internal thermal conductances

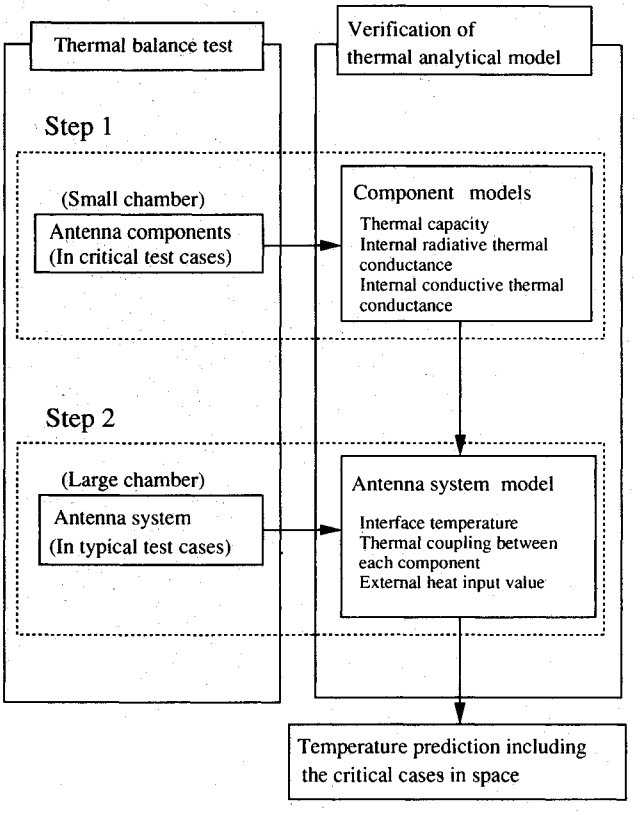

Fig. 6 Two-step thermal design verification method.

Table 2 Properties of thermal control materials

Components	Material	Solar absorptivity,[a] $\alpha_{BOL}/\alpha_{EOL}$	Emissivity,[b] ϵ, ϵ_{eff}
Main reflectors			
Front side	White paint	0.25/0.52	0.82
Back side	MLI (3 layers)	0.44/0.57	0.03*
Subreflectors			
Front side	White paint	0.25/0.52	0.82
Back side	MLI (10 layers)	0.44/0.57	0.015*
Cluster feeds			
Ray path	TC film	0.45/0.45	0.9
Others	MLI (10 layers)	0.39/0.53	0.02*
Antenna tower			
Panel	CFRP		0.8
Truss	CFRP		0.8
Ray path	TC film	0.45/0.45	0.9
Others	Black coated MLI	0.85/0.85	0.81
	(3 layers)		0.03*
	MLI (10 layers)	0.57/0.57	0.015*
APMs	Heaters		
	MLI (10 layers)	0.39/0.53	0.05*
Deployment mechanisms	Heaters		
	MLI (10 layers)	0.39/0.53	0.015*

[a]BOL = beginning of life; EOL = end of experimental mission life (three years).
[b]*denotes ϵ_{eff}, effective emissivity.

for the radiation and conduction. After the thermal balance tests, a temperature cycle test and a soak test were carried out to confirm the antenna's endurance in a space environment. The thermal analytical model of the antenna system was then reconstructed by combining the component thermal analytical models into one unit.

Next, the thermal analytical model of the antenna system was verified by conducting thermal balance tests on the system using typical temperatures test cases. A safe and reliable test configuration and appropriate test cases were selected within the restrictions of the test facility and the size of the antenna module. The test results enabled us to evaluate the thermal coupling between each antenna component, the interface temperatures, and the external heat input values. The temperature difference between the shadowed and the sunlit regions on the front side of the main reflectors adjacent to the antenna tower or the other antenna components were also obtained by using the results of the system test. Then, the thermal analytical model for temperature predictions in the geostationary orbit was verified using the results of this investigation.

Thermal Balance Test

Thermal Analysis Method

The antenna system thermal analytical model was constructed by combining the thermal analytical models of the antenna components to predict the temperatures corresponding to each test case of the system thermal balance tests. The NEVADA[7] (Net Energy Verification and Determination Analyzer) program was used to calculate the radiative thermal conductance and the solar energy absorbed by the antenna module. In determining these factors and quantities, the external surfaces of the antenna module were modeled using plane, spherical, conical, and cylindrical surface elements. The model with 381 nodes, summarized in Table 3, was also developed, and the OLD/SINDA[8] (System Improved Numerical Differencing Analyzer) program was utilized to calculate the temperatures using the lumped parameter method.

Table 3 Number of nodes and thermocouples

Components	Number of nodes[a]	Number of thermocouples[a]
20-GHz-band main reflector	58	57
Reflector, structure	(32)	(31)
MLI	(14)	(6)
Others	(12)	(20)
30-GHz-band main reflector	90	25
Reflector, structure	(26)	(17)
MLI	(22)	(4)
Others	(42)	(4)
Subreflectors	48	26
Reflectors, APMs	(10)	(10)
MLI	(20)	(4)
Others	(18)	(12)
20-GHz-band cluster feed	11	3
30-GHz-band cluster feed	14	3
S-band horn	10	3
C-band horn	9	2
20-GHz/S-bands FSS	4	5
30-GHz/C-bands FSS	4	7
Antenna tower	117	81
Structures	(41)	(36)
MLI	(48)	(30)
Others	(28)	(15)
Supporting structures	14	32
Others	2	8
Total	381	252

[a]( ) denotes subgroup totals.

Antenna Component Thermal Analytical Model

This section presents the modeling method and the improvements in the analytical models obtained from the component thermal balance tests.

Main Reflectors

The external surface data of the 20-GHz-band main reflector is based on the NASTRAN nodal data. The external form model of the reflector front surface was approximated by 56 triangle surfaces, and the analytical model was constructed to divide the surface into 16 nodes. The external form of the 30-GHz-band main reflector front surface was approximated by a part of the spherical surface, and the analytical model was constructed to divide the surface into 14 nodes. The nodes of the truss tubes corresponded to the nodes of the reflector front surface. The detailed analytical models of the deployment mechanisms were adopted for the thermal analytical models of the main reflectors for more accurate temperature predictions of the mechanisms by considering the results of the component thermal balance tests.

Subreflectors and Antenna Pointing Mechanisms

The external form models of the subreflectors and APMs were constructed using a combination of discal, spherical, and cylindrical surfaces. The effective emissivity of MLI blankets for the APMs was modified from 0.02 to 0.05 because of the complicated forms and the heat losses from the uncovered regions of the latch and release mechanisms.

Cluster Feeds

The external forms of the cluster horns were constructed with cylindrical surfaces. Other parts were assembled using a combination of plane surfaces. The conductive thermal conductances between the waveguides and the base plate were modified based on the size of the actual fabricated waveguide supports. Thermal capacities were also modified because of changes in the weight of the cluster feeds.

S-Band Horn

Polygonal planes were used to approximate the external form of the S-band horn. The emissivity of the S-band horn was changed by gold plating the under surface of the horn made of CFRP. The radiative thermal conductance between the under surface and the supporting panel of the S-band horn was also changed for the same reason. Furthermore, conductive thermal conductance between the adjacent nodes at the under surface of the S-band horn was added because unexpectedly large differences between measured and calculated temperatures were observed during the component level tests. The thermal capacity was also modified because of the change in the S-band horn weight.

C-Band Horn

The external form model of the C-band horn was constructed using a combination of conical and discal surfaces. The radiative thermal conductance between the horn and the MLI blankets was verified by the results of the component test because the effective emissivity of the MLI blankets was modified from 0.02 to 0.05 for the complicated form. Then, the conductive thermal conductance between the horn and the flange was modified because a temperature difference of 10°C was measured between these nodes although a difference of only a few degrees was predicted in the analysis. The thermal capacity was also modified because of the change in C-band horn weight.

Frequency Selective Surfaces

The external forms of the FSSs were approximated using a combination of plane surfaces. The typical modification of the thermal properties was the emissivity of the 30-GHz/C-bands FSS because the metal pattern on the surface was modified from the ring type to the ring slot type.

Antenna System Thermal Balance Test

Test Configuration

The 3.5- × 9-m antenna system was tested, and flight models of the main reflectors, subreflectors, and feed components were used. Thermal balance test configuration and test cases were restricted by the antenna size and gravitational deformation of the deployment mechanisms during the test as well as the size of the test facility. Therefore, the thermal balance test was conducted with the aim of obtaining an evaluation of the thermal coupling, which could not be verified by the component thermal balance tests.

The antenna system thermal balance test was performed in a thermal vacuum chamber equipped with a solar simulator. This was done by using the supporting structures that supported the hard points of each main-reflector truss tube just before the latch point to minimize the effect of gravity on the antenna deployment mechanisms. The test setup for the antenna system with supporting structures is shown in Fig. 7.

The antenna system was mounted on a spin table to change the solar beam incident angle. The spin table rotation angle was restricted by the interference of the test fixture and the main reflectors because the antenna system had to be placed within a 6-m solar beam diameter during the thermal balance test. The duration of the thermal balance test was limited to one week due to the time restrictions of the project. Therefore, the operation of the thermal vacuum chamber could not be interrupted during the test if the tests were to be completed on schedule. The test configuration is shown in Fig. 8.

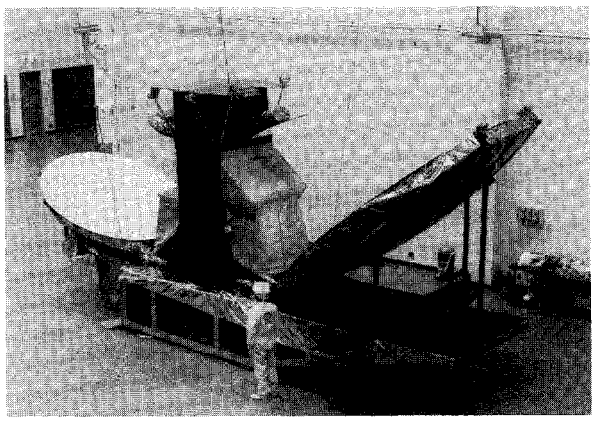

Fig. 7 Test setup for the antenna system.

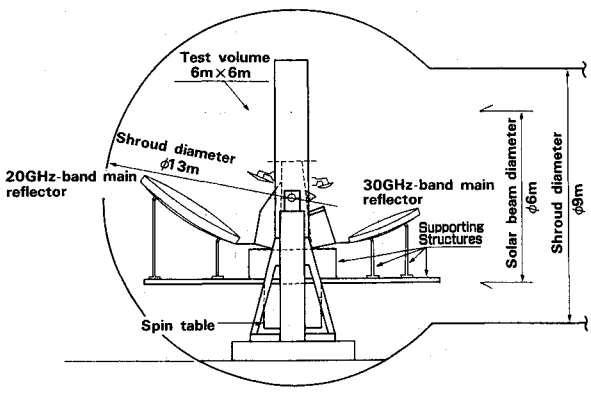

Fig. 8 Test configuration of antenna system.

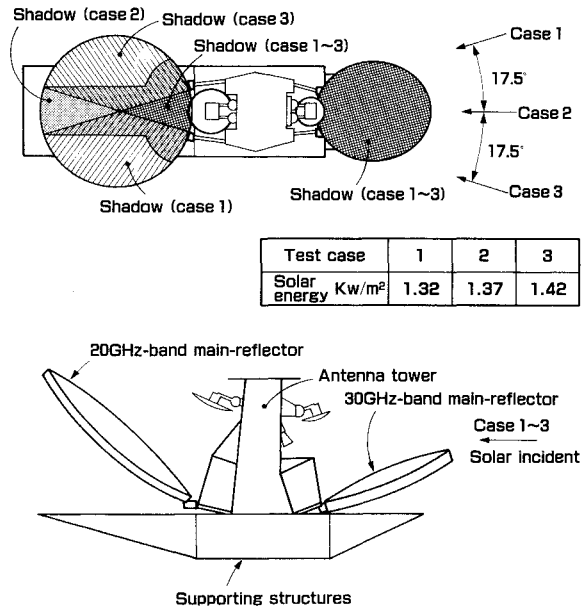

Test case	1	2	3
Solar energy Kw/m²	1.32	1.37	1.42

Fig. 9 Test cases.

Test Conditions

A solar beam was illuminated from the 30-GHz-band main-reflector side to generate a shadow from the antenna tower and the other antenna components on the 20-GHz-band main reflector. The three steady-state test cases shown in Fig. 9 were selected after considering the restrictions mentioned previously.

During the thermal balance test, the chamber shroud was cooled below −180°C by liquid nitrogen, and the chamber pressure was maintained under 1.3×10^{-6} Pa to simulate the thermal vacuum environment of space. The temperatures of the antenna components, the tower truss tubes, and the thermal control materials were measured using C-C type thermocouples at 252 points. A breakdown of the number of thermocouples used is shown in Table 3.

Verification of the Antenna System Thermal Analytical Model

Test Results

The 20-GHz-band main reflector was fixed at a position 9 deg less than the deployment completion position (latch point position) because the reflector had low bending stiffness relative to its weight. Therefore, the solar energy absorbed by the reflector front surface increased from the predicted quantities. The measured temperatures of the 20-GHz-band main reflector were about 20°C higher than the calculated temperatures of the pretest predictions. The measured temperatures of the 20-GHz-band subreflector, which was thermally connected with the 20-GHz-band main reflector through radiation, were also higher than the temperatures calculated before the test.

The front surface of the 30-GHz-band main reflector was not illuminated directly. The reflector was, however, affected by the large amount of thermal radiation from the antenna tower and the front surface of the 20-GHz-band main reflector. The external form model of the 20-GHz-band main reflector that simulated the test configuration was recreated by rotating the reflector 9 deg about the axis through both deployment mechanisms. Then, radiative thermal conductance and solar energy absorbed by the reflector were recalculated using this external surface model.

The supporting structures were designed to decrease the thermal effect on the antenna module. This effect could not be ignored for detailed thermal design verification, however, because of the size (8.5 × 2.0 m) of the supporting structures. Therefore, external form models of supporting structures were created and added to the antenna system thermal analytical model.

Table 4 Calculated and measured temperatures, °C

Components	Items	Case 1	Case 2	Case 3
20-GHz-band main reflector	Calculated	−123 ~ −6	−102 ~ 2	−134 ~ −4
	Measured	−127 ~ 2	−85 ~ 6	−123 ~ 0
	Error	+4 ~ −8	−17 ~ −4	−11 ~ −4
30-GHz-band main reflector	Calculated	−88 ~ −76	−84 ~ −78	−85 ~ −74
	Measured	−74 ~ −61	−71 ~ −65	−73 ~ −60
	Error	−14 ~ −15	−13 ~ −13	−12 ~ −14
20-GHz-band subreflector	Calculated	−69	−83	−61
	Measured	−62	−77	−52
	Error	−7	−6	−9
30-GHz-band subreflector	Calculated	−5	−3	4
	Measured	5	9	14
	Error	−10	−12	−10
20-GHz-band cluster feed	Calculated	−53	−78	−45
	Measured	−48	−70	−39
	Error	−5	−8	−6
30-GHz-band cluster feed	Calculated	−41	−57	−37
	Measured	−28	−57	−31
	Error	−13	0	−6
S-band horn	Calculated	−52	−76	−49
	Measured	−51	−77	−44
	Error	−1	+1	−5
C-band horn	Calculated	37	20	31
	Measured	49	29	45
	Error	−12	−9	−14
20-GHz/S-bands FSS	Calculated	−57/−64	−81/−88	−52/−58
	Measured	−53/−57	−78/−85	−44/−54
	Error	−4/−7	−3/−3	−8/−4
30-GHz/C-bands FSS	Calculated	−7/−20	−22/−35	−13/−26
	Measured	−8/−21	−14/−35	−4/−19
	Error	+1/+1	−8/0	−9/−7

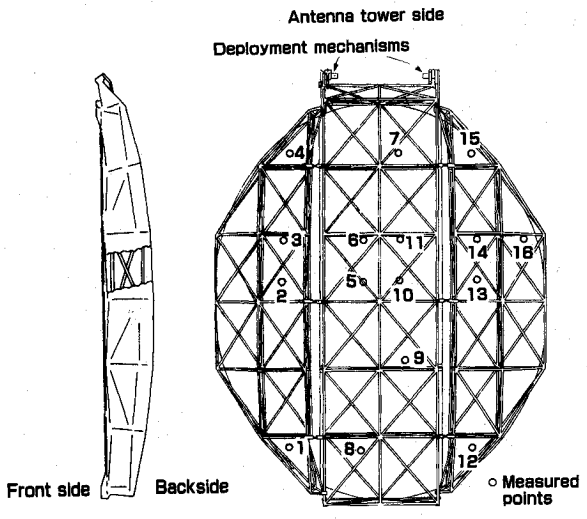

Fig. 10 Measured points on 20-GHz-band main reflector.

Table 5 Comparison between calculated and measured temperatures (20-GHz-band main reflector—case 1)

Measured point (Fig. 10)	Temperature, °C Measured	Calculated
	Shadow region	
1	−127	−123
2	−121	−135
3	−120	−135
4	−114	−124
5	−85	−73
6	−90	−73
7	−76	−44
	Sunlit region	
8	−1	−15
9	−8	
10	−15	−10
11	−23	
12	2	−6
13	−10	−12
14	−14	−12
15	−10	−21
16	−12	−20
	Maximum difference on reflector	
	129	129

Comparison with Prediction

The temperatures, which corresponded to the three test cases, were calculated using the antenna system thermal analytical model. A comparison between the calculated and the measured temperatures of the antenna components is shown in Table 4. The thermal design evaluations of each antenna component, which were based on the results of the antenna system thermal balance test, were as follows.

20-GHz-Band Main Reflector

During the thermal balance test, large temperature gradients across the front surface of the reflector were caused by the shadow of the antenna tower and the other antenna components. The measured points on the 20-GHz-band main reflector are shown in Fig. 10. The calculated and measured temper-

atures on the reflector are shown in Table 5. The measured temperatures were different from the calculated temperatures near the boundary of the shadow and the sunlit region because the reflector front surface thermal analytical model was constructed by dividing the surface into 16 nodes. Good agreement was obtained, however, between the calculated and the measured temperatures at the points away from the boundary, and the difference between the maximum and the minimum temperatures was very small.

30-GHz-Band Main Reflector

The calculated temperatures of the 30-GHz-band main reflector were about 14°C lower than the measured temperatures. The part of the antenna system other than the front surface of the 20-GHz-band main reflector that affected the front surface temperatures of the 30-GHz-band main reflector is most probably the -X side black MLI blanket surface of the antenna tower. The differences between the measured and predicted temperatures of the black MLI blanket surface were from 6 to 39°C. Especially, the measured points on the black MLI blanket near the supports of the 30-GHz-band subreflector and C-band horn showed the large temperature differences because of the multireflections from the sides of the supports, which were wrapped with MLI blankets. Therefore, the thermal analysis was reconducted after putting the boundary at the measured temperatures of the -X side of the antenna tower. The results obtained showed that the calculated temperatures of the front surface of the 30-GHz-band main reflector were about 7°C lower than the measured temperatures.

Thus, it was concluded that the error of the 30-GHz-band main reflector temperature calculation was caused by the antenna tower. However, the external surface temperatures of the antenna tower -X side were not affected by the temperatures of the antenna components other than the 30-GHz-band main reflector. Therefore, it was also concluded that the thermal coupling was adequate between the 30-GHz-band main reflector and the other antenna parts.

Subreflectors

The calculated and the measured temperatures of the 20-GHz-band subreflector showed good agreement, and this result led to the conclusion that the radiative thermal conductance between the subreflector and the 20-GHz-band main reflector was the appropriate value. The measured temperatures of the 30-GHz-band subreflector were about 10°C higher than the calculated temperatures because of the large radiative thermal conductance between the subreflector and the 30-GHz-band main reflector. The results of the previously mentioned analysis, which were reconducted by putting the boundary at temperatures of the -X side of the antenna tower, also showed good agreement (within 6°C) between the calculated and the measured temperatures of the 30-GHz-band subreflector front surface.

Feed Components

The calculated and measured temperatures of the feed components showed good agreement except for the 30-GHz-band cluster feed, C-band horn, and 30-GHz/C-bands FSS. These components were placed on the same side as the 30-GHz-band main reflector and were affected by the temperatures of the reflector front surface. The results, which were described in the analysis of the 30-GHz-band main reflector mentioned earlier, also showed good agreement (within 10°C) between the calculated and the measured temperatures of the 30-GHz-band cluster feed, C-band horn, and 30-GHz/C-bands FSS. Therefore, it was also concluded that the thermal coupling between each antenna component and the solar energy absorbed by the components was the appropriate value.

Table 6 Analysis case of temperature prediction in goestationary orbit

Analysis case	Season BOL/EOL[a]	Solar energy, W/m^2	Temperature of satellite bus, °C
Case A	Equinox, BOL	Sunlit:1353 Eclipse (72 min):0	0
Case B	Summer solstice, EOL	1309	+40
Case C	Winter solstice, BOL	1399	0

[a]BOL = beginning of life; EOL = end of experimental mission life.

Temperature Predictions in Geostationary Orbit

Transient thermal analyses in a geostationary orbit were conducted to predict antenna component temperatures and clarify the temperature margins relative to the in-orbit temperature limits. To treat the extreme thermal environments, the transient thermal analysis was conducted for three periods: the equinox (which included a 72-min period in which the satellite was eclipsed by the Earth), the summer solstice, and the winter solstice, as shown in Table 6.

The solar energy absorbed by the antenna module was calculated using external form models at intervals of 2 h. During the equinox period, additional values were calculated just before entering and after exiting the Earth's shadow. The maximum and minimum temperatures for each antenna component in the three cases analyzed are shown in Fig. 11. The operational and nonoperational temperature ranges of the antenna components are also shown in this figure. This result showed that all antenna component temperatures would be kept within the operational and the nonoperational temperature ranges. Concerning the front surface temperatures of the 30-GHz-band main reflector and the subreflector, the upper temperature margins for the operational ranges were over 10°C even when the temperature prediction errors by the -X side of the antenna tower were considered.

The upper temperature margins were less than 10°C for the operational ranges of the 20-GHz-band cluster feed and the C-band horn, and the lower temperature margin for the operational range of the S-band horn. Therefore, the temperature excursions of these components, shown in Fig. 12, were ex-

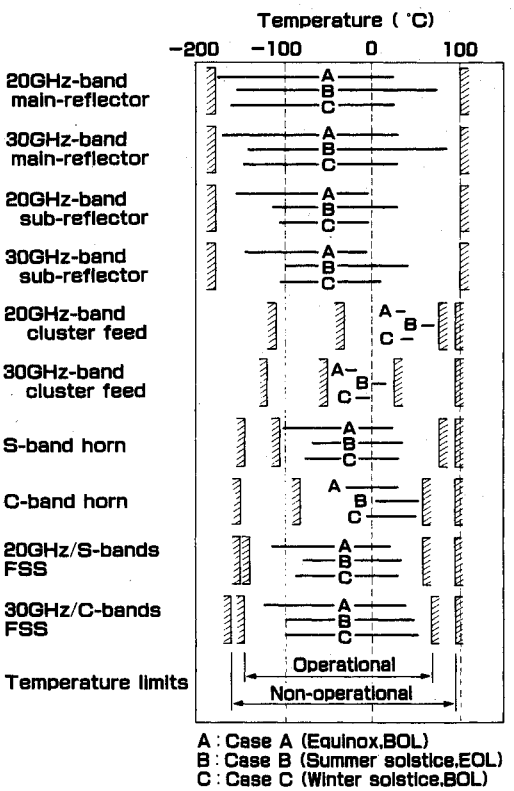

Fig. 11 Geostationary orbit temperature prediction.

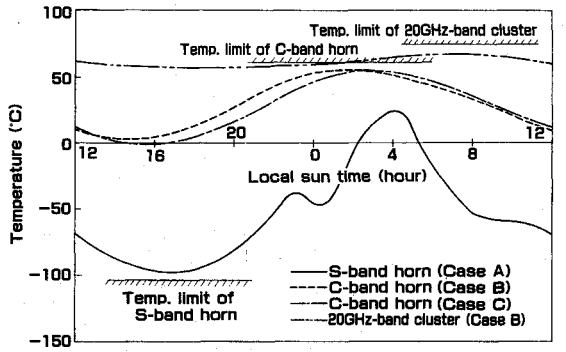

Fig. 12 Temperature excursions of feed components.

amined carefully. As a result, it was concluded that the antenna system thermal design was appropriate because the period of small temperature margins would occur only during a specific period and only for a short duration.

Conclusions

The thermal design and two-step thermal design verification of a large deployable antenna has been described. The results obtained in this study are as follows.

1) The tradeoff study of the thermal control method for main reflectors and the antenna tower indicate that thermal control of the main reflectors can be achieved by applying a combination of white paint and MLI blankets to reduce the temperature swings of the truss structures and by using black MLI blankets to cover the whole antenna tower except for the ray-path area, which is attached to the TC film.

2) For thermal analysis, the chamber shroud temperatures, the deployment angle of the 20-GHz-band main reflector, and the thermal effect of the supporting structures were considered. The calculated temperatures and the results of the thermal balance test showed good agreement except for the 30-GHz-band main reflector, the 30 GHz-band subreflector, and the C-band horn.

3) The surface of the 30-GHz-band main reflector was not illuminated by a solar simulation beam directly, but it had large radiation coupling with the front surface of the 20-GHz-band main reflector, which was illuminated by direct solar beams. Therefore, the temperatures of the 30-GHz-band main reflector were evaluated by considering the deployment angle and the shape of the 20-GHz-band main reflector. The temperatures of the 30-GHz-band subreflector and the C-band horn were evaluated by considering the thermal coupling to the 30-GHz-band main reflector.

4) The agreement between the calculated and the measured temperatures revealed that the temperature requirements of the antenna components were satisfied using the adopted thermal control method.

5) The propriety of the antenna system thermal design was confirmed by thermal analysis using geostationary conditions. It was also confirmed that all antenna components would be maintained within their operational temperature ranges throughout the mission life.

Acknowledgments

The authors wish to express their gratitude for the guidance and encouragement received from Kouzou Morita, Executive Manager of the Radio Systems Laboratory; Syuichi Samejima, Executive Manager of the Satellite Communication Systems Laboratory; and Isao Ohtomo, Research Group Leader of the Satellite Communication Systems Laboratory, NTT Radio Communication Systems Laboratories. Also, thanks are due to Kohei Ohata, Assistant Manager of Mobile Communications Division, NTT (a former member of the NTT Radio Communication Systems Laboratories), with whom we have discussed the thermal design of main reflectors.

References

[1]Ohtomo, I., Kumazawa, T., Kawakami, Y., and Yasaka, T., "Development of the On-Board Fixed and Mobile Multibeam Antenna for ETS-VI Satellite," AIAA Paper 90-0805, March 1990.

[2]Benton, D., "Thermal Control of Large Spacecraft Antenna Reflectors," AIAA Paper 84-1777, June 1984.

[3]Nakajima, K., Nakagawa, K., and Yasaka, T., "Thermal Analysis of a Communication Satellite Antenna," AIAA Paper 81-1092, June 1981.

[4]Spencer, A. L., Monroe, G. A., Schmidt, W. F., and Carton, C., "Intelsat-V Thermal Design, Testing and Flight Performance," AIAA Paper 82-0863, June 1982.

[5]Nakajima, K., and Tsunoda, H., "Study on Thermal Design of Satellite Antenna for Engineering Test Satellite-VI," International Astronautical Federation, Paper 88-040, Oct. 1988.

[6]Horie, T., and Hasuda, Y., "Development of a New Thermal Control Paint for Long-Term Satellites," *IUPAC CHEMRAWN VI, World Conference on Advanced Materials for Innovations in Energy, Transportation & Communications,* Science Council of Japan and Chemical Society of Japan, IIK02, Tokyo, May 1987.

[7]Turner, R. C., "NEVADA User's Manual," Turner Associates Consultants, Incline Village, NV, May 1988.

[8]Gaski, J. D., "OLD/SINDA User's Manual," Network Analysis Associates, Fountain Valley, CA, 1983.

Earl A. Thornton
Associate Editor